catalysts

MDPI

Article

Ligand-Mediated Tuning of Pd-Au Nanoalloys for Selective H_2O_2 Production in Direct Synthesis from H_2 and O_2

Tingting Hu [1], Baozeng Ren [1,*] and Liang Zhao [2,3,*]

[1] School of Chemical Engineering, Zhengzhou University, Zhengzhou 450001, China; hutingting1011@126.com
[2] Max Planck-Cardiff Centre on the Fundamentals of Heterogeneous Catalysis FUNCAT, Cardiff Catalysis Institute, School of Chemistry, Cardiff University, Cardiff CF10 3AT, UK
[3] BASF Advanced Chemicals Co., Ltd., Shanghai 200137, China
* Correspondence: renbz@zzu.edu.cn (B.R.); zhaol28@cardiff.ac.uk (L.Z.)

Abstract: Hydrogen peroxide (H_2O_2) is an important industrial chemical that is widely applied in many areas. The direct synthesis of H_2O_2 from H_2 and O_2 has proved to be a green and economic pathway. Pd-based bimetallic catalysts, due to their superior catalytic performances in this reaction, have attracted intensive attention. Herein, Tetrakis(hydroxymethyl)phosphonium chloride (THPC) was adopted as the protective ligand to immobilize Pd-Au alloy nanoparticles onto activated carbon (AC). The varied Pd/Au molar ratios demonstrated homogeneously distributed Pd-Au nanoalloys with average particle sizes ranging from 3.51 to 5.75 nm. The optimal ratio was observed over the Pd_3Au_1/AC-THPC catalyst with a maximum H_2O_2 productivity of 165 mol/($kg_{Pd}\cdot$h) and selectivity of 82.3% under ambient pressure. The relationship between the electronic structure and catalytic activity indicated Pd^0 was the active site, while the presence of Au inhibited H_2O_2 degradation rate. This research could help in the design efficient bimetallic catalysts for the direct synthesis of H_2O_2.

Keywords: H_2O_2 synthesis; Pd-Au alloy; THPC; high H_2O_2 selectivity

1. Introduction

Hydrogen peroxide (H_2O_2) is a crucial industrial chemical with diverse applications, ranging from its use as a bleaching agent in the paper and textile industries to its role as a disinfectant, oxidizer, and in the production of chemicals such as peracetic acid [1–4]. Additionally, it has potential applications in green chemistry, environmental remediation, and energy storage [2–4]. The dominant method for industrial H_2O_2 production is the anthraquinone oxidation (AO) process, which relies on the hydrogenation of anthraquinone to form hydrogenated derivatives, followed by oxidation with oxygen to regenerate the anthraquinone. This process is generally carried out in large-scale facilities due to its complexity and the significant use of solvents [1–6].

In recent years, there has been a shift towards the direct synthesis of H_2O_2 from H_2 and O_2, which could theoretically eliminate the need for complex intermediates and toxic solvents [2,5–7]. However, this approach faces significant challenges due to the difficulty of selectively activating O_2 while minimizing side reactions, such as the production of water or other reactive oxygen species, which would lower the efficiency of H_2O_2 production [2]. This is where advances in catalysis become pivotal, as catalytic systems can lower activation energy and enable more controlled reactions. Over the past few decades, significant progress has been made in developing novel catalytic systems that facilitate this reaction

Academic Editor: Mauro Bassetti

Received: 13 April 2025
Revised: 19 May 2025
Accepted: 27 May 2025
Published: 30 May 2025

Citation: Hu, T.; Ren, B.; Zhao, L. Ligand-Mediated Tuning of Pd-Au Nanoalloys for Selective H_2O_2 Production in Direct Synthesis from H_2 and O_2. *Catalysts* **2025**, *15*, 544. https://doi.org/10.3390/catal15060544

under mild conditions, with minimal by-products. Various catalytic materials, including noble metals, metal oxides, and carbon-based materials, have been explored [5,8–10].

Pd-based catalysts have been widely used in the direct synthesis of H_2O_2 due to their unique catalytic properties [2,10,11]. They can adsorb and dissociate H_2 molecules while exhibiting a certain degree of selectivity for H_2O_2 formation, rather than fully oxidizing hydrogen to form water (H_2O), which is a common competing reaction [2,10]. However, achieving high selectivity for H_2O_2 generation remains challenging, as pure Pd catalysts tend to fully oxidize H_2 to H_2O. Therefore, studies on Pd-based catalysts often involve modifications or combinations with other elements or supports to enhance their selectivity, activity, and stability [12].

One significant breakthrough in this field over the years has been the incorporation of Au into supported Pd-based catalysts, forming Pd-Au alloy catalysts [13]. In the direct synthesis of H_2O_2, the unique role of Pd-Au alloy catalysts is manifested in several ways [13–15]: (1) Enhanced selectivity: Pure Pd catalysts often over-oxidize H_2 to form H_2O, which reduces H_2O_2 productivity. The addition of Au can adjust the surface electronic properties of Pd, making its surface active sites more selective for H_2O_2, thereby reducing water formation. This selectivity enhancement is related to the electronic and geometric effects on the Pd-Au surface. (2) Improved catalytic activity: the formation of Pd-Au alloy catalysts increases the catalyst's activity. The interaction between Au and Pd results in surface active sites with higher catalytic potential, helping to more effectively activate reactant molecules (H_2 and O_2) and thus promote H_2O_2 generation. (3) Improved stability: Compared with pure Pd catalysts, Pd-Au alloys exhibit higher stability in long-term reactions. They are less prone to deactivation and possess better antioxidant and anti-aggregation properties under reaction conditions, thus extending the catalyst's lifespan. Professor Graham J. Hutchings and his research group at Cardiff University have made outstanding contributions to the field of direct H_2O_2 synthesis, particularly in the development and optimization of Pd-Au alloy catalysts [2,13]. They were among the first teams to discover that Pd-Au alloy catalysts exhibit significant selectivity and high activity for direct H_2O_2 synthesis [7,16]. Through the synergistic effect between Au and Pd, they demonstrated that Au can significantly inhibit the complete oxidation pathway of Pd catalysts, thereby increasing the selectivity for H_2O_2. Their research revealed the unique advantages of Pd-Au catalysts and explored the high selectivity and high activity of these catalysts in direct H_2O_2 synthesis [13].

Pd-Au alloy catalysts have demonstrated superior activity and selectivity in the direct synthesis of H_2O_2 from hydrogen and oxygen. Consequently, the preparation of Pd-Au alloy catalysts with uniform size and morphology becomes crucial. The conventional and simple impregnation method was initially used to prepare Pd-Au catalysts; however, this method often fails to achieve a uniform alloy phase, and the calcination process can easily cause nanoparticle (NP) aggregation, negatively impacting catalyst performances [17–20]. The sol-immobilization method, on the other hand, can produce uniformly distributed Pd-Au nanoalloys with a narrow particle size distribution (PSD), making it particularly suitable for studying catalytic reactions [11,21]. The most commonly applied protective agents in the sol-immobilization method are poly(vinyl alcohol) (PVA) and poly(vinyl pyrrolidone) (PVP) [11,22–24]. However, the remaining PVA and PVP can have positive effects in the productivity, catalytic activity, and selectivity, thus hindering the investigation and interpretation of the catalytic active sites and catalytic nature [25,26]. Tetrakis(hydroxymethyl)phosphonium chloride (THPC) as a reducing and stabilizing agent has also been used in the synthesis of small metal NPs with a narrow PSD, especially for noble metals such as Au, Pd, and Pt [27,28]. Moreover, regarding the THPC method, it has not been reported that its presence over the metal NPs would make an impact on the catalytic performances.

In this research, the sol-immobilization method using the THPC agent was adopted for the preparation and investigation of Pd-Au alloy NPs over activated carbon (AC) material. The AC was selected as the support due to its high specific surface area (SSA) and abundant acidic sites. These acidic sites on the carbon support surface can inhibit the further decomposition of the generated H_2O_2, thus increasing its selectivity [15]. Further investigations were focused on the Pd/Au molar ratio effect on the structural and electronic modifications and how these modifications influence the catalytic performances in the direct synthesis of H_2O_2.

2. Results and Discussion

2.1. Structural Properties of Pd_xAu_y/AC-THPC

Four bimetallic Pd_xAu_y/AC-THPC catalysts were synthesized using the sol-immobilization method with varied Pd/Au ratios (1/1, 2/1, 3/1 and 4/1).

Figure 1 shows the transmission electron microscopy (TEM) images and the particle size distribution (PSD) of the metal NP sizes for Pd_xAu_y/AC-THPC catalysts with different Pd/Au ratios. From the TEM images, it can be observed that small metal NPs were uniformly distributed on the AC support with a narrow PSD. The average NP size of the Pd_xAu_y/AC-THPC catalysts increased gradually with the Pd/Au ratio, from 3.51 nm over Pd_1Au_1/AC-THPC to 5.75 nm over Pd_4Au_1/AC-THPC. This may be due to the insufficient amount of THPC added in the preparation of Pd-Au/AC-THPC catalysts with higher Pd/Au ratios, which results in less effective control over the PSD. Nevertheless, notably, the THPC-stabilized NPs supported on Pd-Au/AC-THPC catalysts demonstrated a significantly narrower PSD ($\pm$0.9 nm) compared to their ligand-free Pd-Au/Al_2O_3 counterparts ($\pm$2.4 nm), as quantified in Supplementary Figure S1. This disparity in monodispersity highlights the critical influence of THPC coordination chemistry in suppressing nanocristal agglomeration during NP synthesis. Interestingly, by measuring the lattice fringes of the nanoparticles, we can easily observe the Pd (111) lattice fringes with an interplanar spacing of 0.23 nm [29]. This indicates that in Pd-rich (Pd/Au $\geq$ 1) Pd-Au/AC-THPC catalysts, the Pd component is still more easily identified, while the elemental distribution of Au requires other methods for detection.

To further characterize the elemental distribution of Pd and Au, as well as the chemical composition of the metal NPs in the Pd-Au/AC-THPC catalyst, aberration-corrected scanning transmission electron microscopy (AC-STEM) and energy dispersive x-ray (EDX) spectroscopy were employed (Figure 2). The EDX mapping images (Figure 2(a_1,a_2,b_1,b_2)) and EDX spectra (Figure S2) reveal that the metal NPs were uniformly dispersed on the carbon support, with the elemental distributions of Pd and Au nearly overlapping and both elements being present on each individual NP. This observation directly demonstrates that the THPC method successfully produced uniformly distributed and randomly arranged Pd-Au alloy NPs. In addition, the C signal (Figure 2(a_3,b_3)) originated from the AC support, while the O signal (Figure S2) can be attributed to oxygen-containing species on the surface of the activated carbon (such as hydroxyl and carboxyl groups) as well as the oxidized state of the metal on the catalyst surface [30].

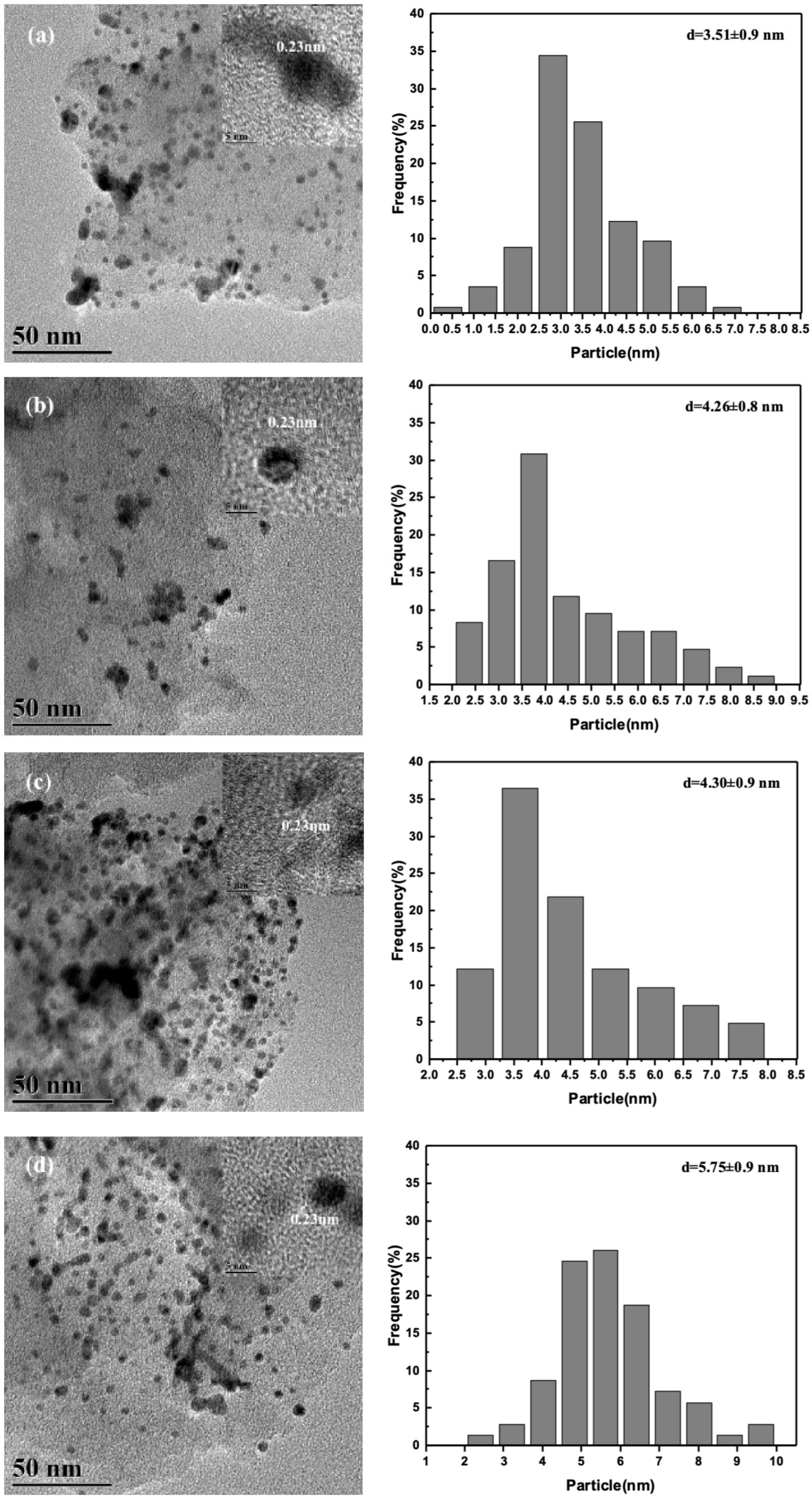

Figure 1. TEM micrographs and particle size histograms of (**a**) Pd_1Au_1/AC-THPC, (**b**) Pd_2Au_1/AC-THPC, (**c**) Pd_3Au_1/AC-THPC, and (**d**) Pd_4Au_1/AC-THPC catalysts.

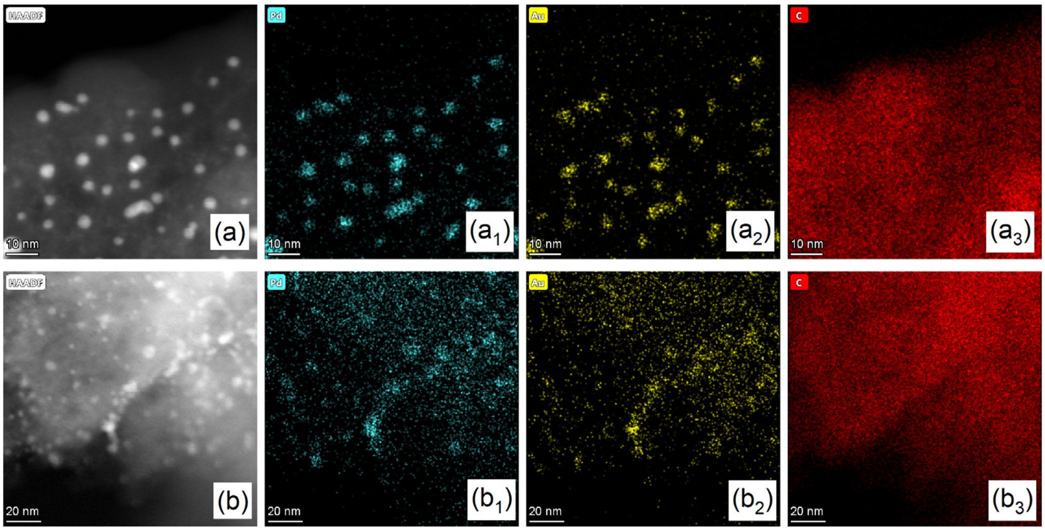

Figure 2. HAADF-STEM and EDX mapping images of (**a**) Pd_2Au_1/AC-THPC and (**b**) Pd_3Au_1/AC-THPC catalysts. (**a_1–a_3**) elemental distributions of Pd, Au and C over Pd_2Au_1/AC-THPC catalyst and (**b_1–b_3**) elemental distributions of Pd, Au and C for Pd_3Au_1/AC-THPC catalyst.

The XRD technique was adopted to investigate the crystalline structure of bimetallic Pd-Au/AC-THPC catalysts with the varied Pd/Au ratios, as shown in Figure 3. The XRD patterns of these catalysts exhibit three main characteristic diffraction peaks located at 2θ = 24.3°, 39°, and 43.3°. The first two peaks correspond to the characteristic reflections of C (002) and C (101), respectively [31]. The peak at 39° can be attributed to the mixed-metallic components of Pd and Au [32]. According to the literature, the Pd(111) and Au(111) planes are located at 40.1° and 38.3°, respectively. Furthermore, STEM-EDX images (Figure 2) confirm that Pd and Au coexist within the same NPs. Therefore, the characteristic diffraction peak at 2θ = 39° should be ascribed to the Pd-Au alloy phase, consistent with reported XRD peak positions in the literature [32,33]. Variations in the intensity of the Pd-Au alloy peak among different catalysts may be related to differences in the sample amount used during testing or the actual metal loading of the catalysts.

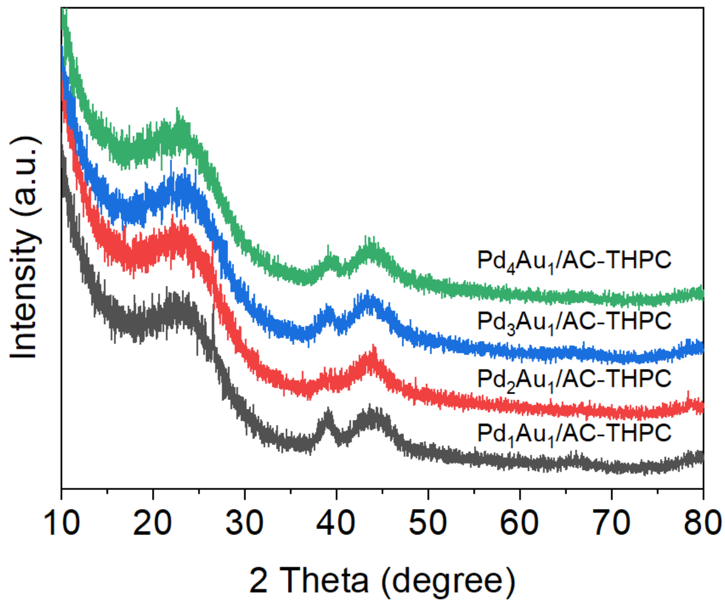

Figure 3. XRD patterns of Pd_xAu_y/AC-THPC catalysts with the variation of Pd/Au molar ratios.

The results for the specific surface area (SSA), pore volume, and pore size distribution of the catalysts are presented in Figure 4 and Table 1. All the synthesized catalysts demonstrated SSAs in the range of 1000–1100 m^2/g, suggesting that the Pd/Au ratio has no significant impact on the SSA. At low P/P_0 values, the N_2 adsorption increased rapidly with an initial rise in P/P_0 and then increased more gradually. At higher P/P_0 values, the N_2 adsorption stabilized, reaching a constant value. This behavior indicated that the nitrogen adsorption of the AC-supported Pd-Au bimetallic catalysts followed a microporous adsorption–desorption isotherm. The strong interactions between nitrogen molecules and the adsorbent in the low-pressure region led to substantial nitrogen adsorption. The pore volume and the average pore size of the catalyst samples exhibited minimal variation, remaining within the range of 0.56–0.58 cm^3/g and the range of 3.13–3.18 nm.

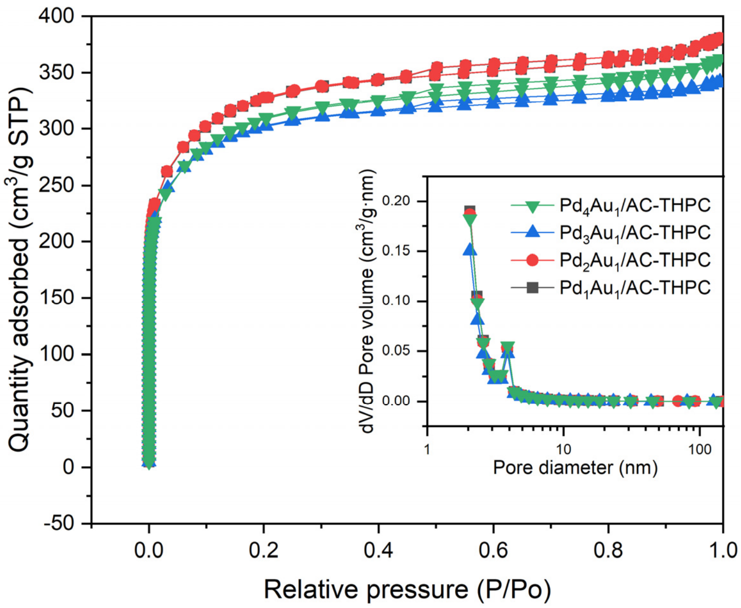

Figure 4. Adsorption/desorption of N_2 isotherm profile for Pd_xAu_y/AC-THPC catalysts with the variation of Pd/Au molar ratios.

Table 1. Textual properties of Pd_xAu_y/AC-THPC catalysts with the variation of Pd/Au molar ratios.

Catalyst	SSA (m^2/g)	Pore Volume (cm^3/g)	Average Pore Size (nm)
Pd_1Au_1/AC-THPC	1087	0.589	3.18
Pd_2Au_1/AC-THPC	1088	0.588	3.17
Pd_3Au_1/AC-THPC	1053	0.573	3.13
Pd_4Au_1/AC-THPC	1027	0.561	3.15

As shown in Figure 5a, the XPS spectrum of each PdAu/AC-THPC catalyst exhibits three characteristic peaks in the Pd 3d region. Taking Pd_1Au_1/AC-THPC as an example, these peaks are located at 337.9 eV, 335.9 eV and 335.4 eV, corresponding to Pd^{2+} $3d_{5/2,}$ Pd^0 $3d_{5/2,}$ and Au $4d_{5/2}$, respectively. Figure 5c demonstrated a composition-dependent modulation of palladium oxidation states, with the surface Pd^{2+} fraction decreasing linearly (R^2 = 0.94) as the Pd/Au molar ratio increases, while the Pd^0 content exhibits a proportional rise (R^2 = 0.91). This inverse correlation directly correlates with Pd-Au alloy formation, wherein d-orbital hybridization between Pd and Au alters the electron density of Pd orbitals [17]. Correspondingly, the Au 4f XPS spectra reveal a systematic negative binding energy shift (Δ = 0.1–0.3 eV) in Au^0 $4f_{7/2}$ and Au^0 $4f_{5/2}$ peaks (Figure 5b), consistent with electron transfer from Pd to Au driven by Au's higher electronegativity [33]. These parallel trends in Pd and Au electronic states mechanistically confirm alloy-induced interfacial charge redistribution.

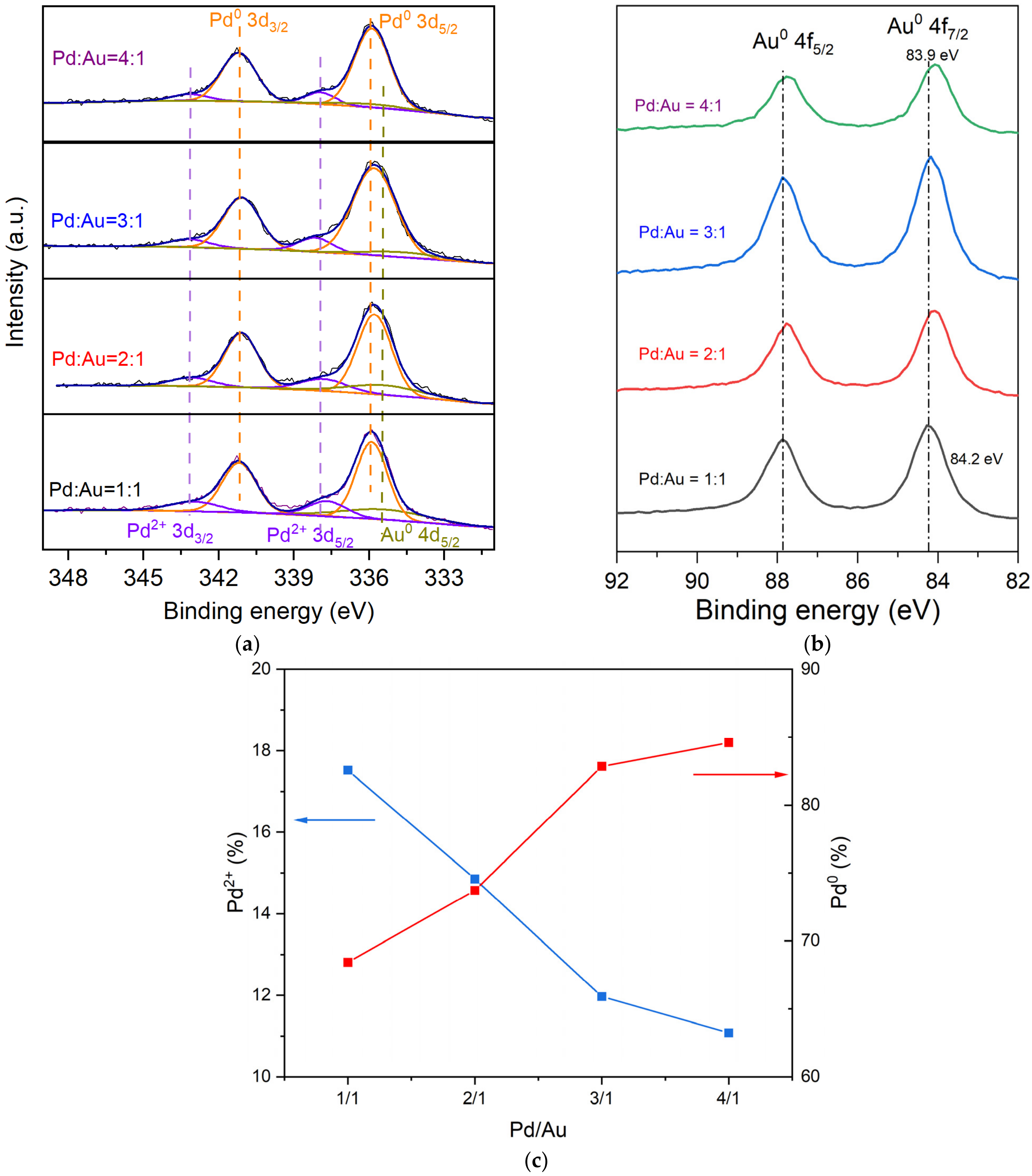

Figure 5. Pd 3d (**a**) and Au 4f (**b**) spectra from XPS experiments conducted over Pd_xAu_y/AC-THPC catalysts with the variation of Pd/Au molar ratios. (**c**) Surface chemical composition of Pd^{2+} (blue) and Pd^0 (red) derived from XPS spectra of Pd_3Au_1/AC-THPC catalyst.

2.2. Catalytic Performance of Pd_xAu_y/AC-THPC

The above characterization results demonstrated the formation of Pd-Au alloy over AC support, modifying the electronic structures of Au and Pd. The catalytic activity of Pd_xAu_y/AC-THPC catalysts was then evaluated in the direct synthesis of H_2O_2

from H_2 and O_2 and compared with reported Pd-based catalysts (Table 2). Notably, at 10 min reaction, the Pd_3Au_1/AC-THPC catalyst exhibited the highest H_2O_2 productivity (165 mol/(kg_{Pd}·h)) and H_2O_2 selectivity (82.3%) in this research. However, these values dropped to 71 mol/(kg_{Pd}·h) and 35.9%, still outperforming the other Pd_xAu_y/AC-THPC catalysts. Among these catalysts, Pd_xAu_y/AC-THPC catalysts of Pd/Au = 3/1 and 4/1 seem to display higher activity than those of Pd/Au = 1/1 and 2/1. As shown in Figure 5, Pd_3Au_1/AC-THPC and Pd_4Au_1/AC-THPC catalysts possessed more Pd^0 (82.8% and 84.6%, respectively) than the other two catalysts of 1/1 and 2/1 (68.4% and 73.7%, respectively), possibly suggesting Pd^0 is the active valence state of Pd. With the increase in the Au molar fraction, the H_2O_2 degradation rate over Pd_1Au_1/AC-THPC (425 mol/(kg_{Pd}·h)) was observed to be lower than that over Pd_3Au_1/AC-THPC (723 mol/(kg_{Pd}·h)), which is consistent with the reported literature. These demonstrated that, for Pd-Au alloy catalysts prepared via the THPC method, the catalytic performance is optimal when the Pd/Au ratio is 3/1. Pd-Au alloy catalysts typically exhibit the best performance at an optimal Pd/Au ratio, which is attributed to the synergistic effect between Pd and Au. According to the literature, Pd exhibits strong adsorption, activation, and conversion abilities for H_2 and O_2, but these same properties make monometallic Pd catalysts more prone to overreaction, leading to the formation of H_2O rather than H_2O_2. The introduction of Au weakens Pd's adsorption and desorption of intermediate species, optimizing the reaction pathway and favoring the formation of H_2O_2, thereby increasing selectivity [34]. Moreover, Flaherty et al. [14,34] demonstrated that this improvement is primarily due to the electronic structure optimization between Pd and Au. However, over time, the selectivity for H_2O_2 gradually decreases, likely due to the further decomposition of the produced H_2O_2 into water.

Table 2. Catalytic performances in the direct synthesis of H_2O_2 from H_2 and O_2.

Catalyst	Time (min)	Solvent	Temperature (°C)	Pressure (bar)	H_2O_2 Productivity mol/(kg_{Pd}·h)	H_2O_2 Selectivity (%)
Pd_1Au_1/AC-THPC	30	EtOH/H_2SO_4	10	1	18	3.8
Pd_2Au_1/AC-THPC	30	EtOH/H_2SO_4	10	1	14	5.3
Pd_3Au_1/AC-THPC	10	EtOH/H_2SO_4	10	1	165	82.3
Pd_3Au_1/AC-THPC	30	EtOH/H_2SO_4	10	1	71	35.9
Pd_3Au_1/AC-THPC	60	EtOH/H_2SO_4	10	1	42	6.0
Pd_4Au_1/AC-THPC	30	EtOH/H_2SO_4	10	1	56	19.5
Pd_4Au_1/AC-THPC	60	EtOH/H_2SO_4	10	1	45	5.7
$Pd_{2.5}Au_{0.5}/TiO_2$ [35]	30	EtOH/H_2SO_4	10	1	2069	46.0
$Pd_{0.5}Au_{2.5}/TiO_2$ [35]	30	EtOH/H_2SO_4	10	1	774	38.5
Pd/HAP [36]	30	EtOH/H_2SO_4	10	1	741	43
$Pd_{40}Ag_1$/AC [37]	15	MeOH/H_2SO_4	2	30	7022	71
$Pd_1Au_1/CeZrO_x$ [38]	180	MeOH/H_2SO_4	20	1	1270	61
Pd_1Au_1/AC [15]	30	MeOH/H_2O	2	37	320	95
Pd_3Au_1/SiO_2 [39]	150	MeOH/HCl	10	1	1770	63
Pd_1Zn_9/Al_2O_3 [40]	15	MeOH/H_2SO_4	2	30	25,431	78.5
Pd_2Ga/TiO_2 [41]	30	MeOH/H_2O	2	29	4269	30

Reaction conditions: 60 mL solvent (ethanol/H_2SO_4), 60 mL/min ($H_2/O_2/N_2$ = 9/36/15), 50 mg, 1 bar, 10 °C, and stirring rate = 1000 r/min.

In order to further investigate the catalytic activity and stability of the Pd_3Au_1/AC-THPC catalyst, additional results were presented in Figure 6. In Figure 6a, a rapid accumulation of H_2O_2 was observed within the initial 10-min reaction period, demonstrating the catalyst's superior activation kinetics. Maximum H_2O_2 selectivity and productivity were attained at 10 min (Table 2), corresponding to optimal surface active-site utilization before competitive degradation pathways became thermodynamically favorable. With the reaction time going, though H_2O_2 concentration was increasing over time, the H_2O_2 productivity and selectivity declined due to the high degradation rate, which can be supported by its high excellent reusability with three cycles of reaction running. The high catalyst stability validated the analysis and comparison of catalytic performances.

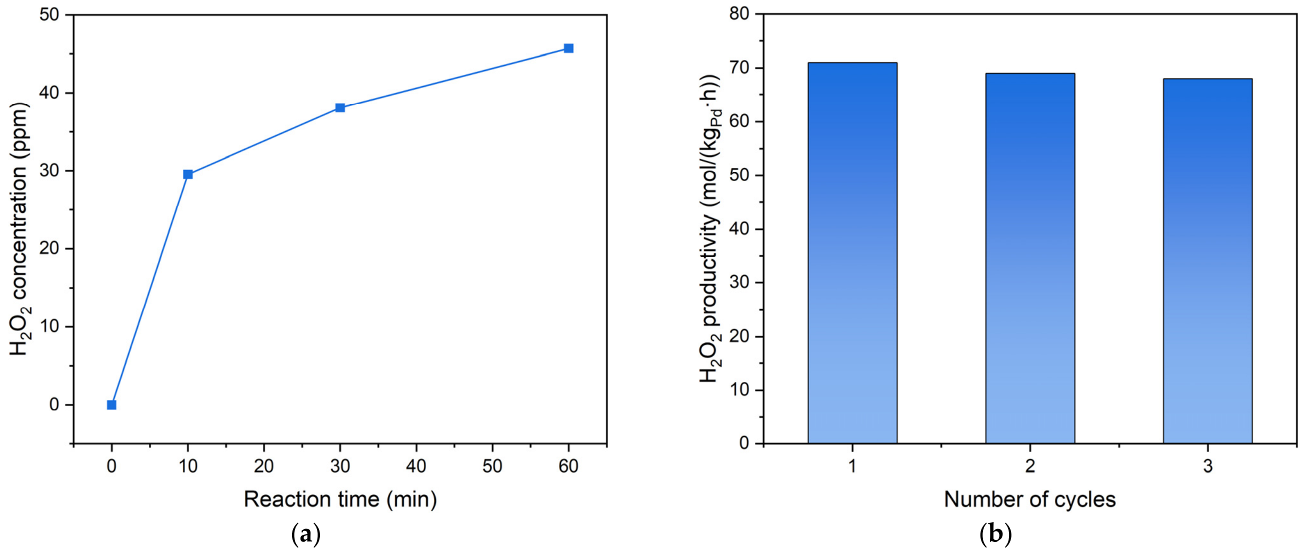

Figure 6. Temporal evolution of H_2O_2 concentration during the catalytic reaction (**a**) and the reusability test (**b**) over Pd_3Au_1/AC-THPC for the direct synthesis of H_2O_2. Reaction conditions: 60 mL solvent (ethanol/H_2SO_4), 60 mL/min ($H_2/O_2/N_2$ = 9/36/15), 50 mg, 1 bar, 10 °C, stirring rate = 1000 r/min, and reaction time: as stated (**a**) and 30 min (**b**).

The catalytic performances of the reported Pd-based catalysts in the direct synthesis of H_2O_2 were presented in Table 2. It can be observed that our Pd_3Au_1/AC-THPC catalyst exhibits a selectivity comparable to that reported in the literature, with only the Pd_1Au_1/AC catalyst reported by Prof. Hutchings showing a higher selectivity of 95% under the conditions of 2 °C and 37 bar, which surpasses our 82.3% [15]. However, when comparing H_2O_2 productivity, it is evident that the catalysts reported in the literature achieve significantly higher productivity than ours. Under these optimized reaction conditions, the further decomposition of H_2O_2 can be largely suppressed, thus improving the selectivity and productivity [42]. In addition, pre-treatment using acid on the support would also dramatically enhance the H_2O_2 productivity. However, in this research, the reactions were conducted at 1 bar and 10 °C. The high degradation rate (723 mol/(kg$_{Pd}$·h)) of H_2O_2 vs. the maximum productivity (165 mol/(kg$_{Pd}$·h)) under these reaction conditions supports our hypothesis.

Therefore, to enhance the H_2O_2 productivity of Pd_xAu_y/AC-THPC catalysts, further optimization of the reaction conditions will be required in future work. Given that the aim of this study was to prepare uniform and stable Pd-Au alloy catalysts with THPC and investigate the effect of the Pd/Au ratio on the catalytic performance of Pd-Au alloy catalysts, our work would provide valuable insights for the design of efficient bimetallic catalysts for the direct synthesis of H_2O_2.

3. Materials and Methods

3.1. Chemicals and Materials

$PdCl_2$, Palladium Chloride (Sigma-Aldrich, China, ≥99%); $AuCl_3 \cdot HCl \cdot 4H_2O$, Chloroauric Acid (Damas-beta, China, 99%); THPC, Tetrakis(hydroxymethyl)phosphonium chloride (Aladdin, China, 0.5%); NaOH, Sodium Hydroxide (Sinopharm Chemicals, China, >96.0%); C_2H_5OH, EtOH (Sinopharm Chemicals, China, >99.7%); H_2SO_4, Sulfuric Acid (Sinopharm Chemicals, ≥95%); AC, activated carbon (Guangzhou Changyu Chemical, China, 99.999%); Molecular H_2 (Jining Xieli Special Gas, China, 99.999%), Molecular O_2 (Jining Xieli Special Gas, China, 99.999%); and Molecular N_2 (Jining Xieli Special Gas, China, 99.999%)

3.2. Catalyst Preparation

3.2.1. Pd-Au/AC-THPC Catalysts

Typically, 0.3 mL of 0.1 mol/L NaOH solution measure was added to 45 mL of deionized water in a beaker, followed by 1.2 mL of a 10 mg/mL THPC aqueous solution under continuous stirring. After 10 min, calculated quantities of Au and Pd precursor solution were added to the above beaker. During the reaction, the color of the solution changes from brownish-yellow to dark brown. After 15 min of reduction, 1 g of AC support was added and followed by 3–4 drops of H_2SO_4. The slurry was stirred for 2 h and then filtered and washed with 1.5 L of deionized water to remove residual ions. The filtrate should be colorless, indicating that the NPs are fully loaded onto the support. After washing, the resulting material was moved to the drying oven at 100 °C for 12 h to obtain the final catalyst sample. The catalysts were denoted as Pd_xAu_y/AC-THPC, where x/y represents the molar ratio of Pd/Au, e.g., Pd_2Au_1/AC-THPC.

3.2.2. Pd-Au/Al_2O_3 Catalyst

Typically, calculated amounts of Au and Pd precursor solution were added to 100 mL DI water under rigorous stirring. After 10 min, 1 g of Al_2O_3 powder was added and the slurry was kept stirring for another 1 h. Before transferred to the 100 °C drying oven, the paste was obtained through filtration and a washing process. The resulting catalyst was collected after calcination in air at 400 °C for 3 h.

3.3. Catalyst Testing

Direct hydrogen–oxygen synthesis of H_2O_2 is a typical gas–liquid–solid three-phase reaction. The gas is introduced from the bottom, dispersed through a sintered glass filter, and then participates in the reaction with the solvent. After the reaction, the gas passes through an online chromatographic detector. Due to the explosive nature of H_2 (4–75%), N_2 is used for dilution and protection ($H_2/O_2/N_2$ = 9/36/15 (vol)), which also serves as an internal standard for the quantitative analysis of H_2 and O_2 gas concentrations. The total flow rate is controlled at 60 mL/min. In order to further ensure the experimental safety, the flame-free operational regulation is implemented in the lab. Magnetic stirring is employed to enhance the dispersion of catalyst suspension particles. The reactor is equipped with a jacket for temperature control during the reaction.

The experiment involves the direct synthesis of H_2O_2 from H_2 and O_2. H_2O is used as the mobile phase, and a specifically designed high-temperature, high-pressure fixed-bed reactor system is set up to meet these conditions. Raw gases and H_2O are introduced from the bottom of the reactor to react with the catalyst to produce H_2O_2. As H_2O exits the reactor, H_2O_2 is carried out and separated via a gas–liquid separator. The exhaust gas then enters the gas chromatograph and gas mass spectrometer for the online detection of gas composition and concentration. The H_2O_2 concentration in the liquid phase is subsequently measured by a UV spectrophotometer.

H_2O_2 selectivity and H_2O_2 productivity were calculated according to the following equations:

$$H_2O_2 \text{ selectivity } (\%) = \frac{mol\ of\ H_2O_2}{mol\ of\ converted\ H_2} \times 100\% \quad (1)$$

$$r_{H_2O_2} = \frac{c_{H_2O_2} \times F_{H_2O}}{m_{cat} \times S_{Pd} \times Dis_{Pd} / M_{Pd}} \quad (2)$$

where $c_{H_2O_2}$ is the concentration of H_2O_2, mol/L; F_{H_2O} is flow rate of water, L/s; m_{cat} is the catalyst mass, g; S_{Pd} is the Pd loading, wt%; Dis_{Pd} is the Pd dispersion; and M_{Pd} is the molecular weight of Pd, g/mol.

3.4. Catalyst Characterisation

XRD measurements were performed using a Bruker D8 Advance instrument with the following conditions: voltage 40 kV, current 40 mA, Cu-Kα radiation source (λ = 1.54056 Å), diffraction range 10–80°, and a typical scanning speed of 0.4 °/min.

The SSAs and pore volumes of the catalysts were measured using the Micromeritics ASAP-2460 automatic rapid surface area analyzer (Micromeritics Instrument Corporation, Shanghai, China). The measurement conditions were as follows: the catalyst samples were placed in a vacuum oven and dried at 50 °C for 72 h. Prior to measurement, the samples were degassed with nitrogen at 100 °C for 12 h. The specific surface area of the catalysts was then determined at −196 °C.

AC-STEM was performed using a TECNAI G2 F20 transmission electron microscope manufactured by FEI (Hillsboro, OR, USA). The measurement conditions were as follows: working voltage of 200 kV. The samples were thoroughly ground and dispersed in anhydrous ethanol for 1 h of ultrasonication. Afterward, a droplet of the clear middle liquid was placed on a copper grid using a pipette, and the sample was left to dry as the ethanol evaporated before being placed in the sample chamber.

The average particle size (d) of the catalyst was calculated using Equation (3):

$$d = \frac{\sum n_i d_i^3}{\sum n_i d_i^2} \quad (3)$$

where n_i represents the number of catalyst particles with a diameter d_i, and d_i represents the particle size of the catalyst. i represents the total number of particles in the image.

XPS is used to determine the types and oxidation states of elements, primarily for studying the elemental composition and various oxidation states at the surface of materials. In this study, XPS analysis was performed using an ESCALAB250Xi system (Thermo Fisher Scientific, Shanghai, China) to analyze the electronic environment of the surface elements of the catalyst. The test used an Al-Kα radiation source (1486.6 eV, with a pass energy of 30.0 eV). Binding energies were calibrated based on the position of the C 1s peak at 284.8 eV, and the spectra were analyzed following references from the literature.

4. Conclusions

The direct synthesis of H_2O_2 from H_2 and O_2 is an atom-efficient approach compared to the industrial production process. Herein, THPC, the protective-ligand, stabilized Pd-Au alloy NPs were immobilized onto AC support for this reaction. STEM-EDX confirmed composition-tunable Pd-Au nanoalloys with uniform homogeneous distribution and controlled particle sizes via THPC stabilization. The strong interaction between Pd and Au within alloy NPs modified their electronic structures, exhibiting the optimal ratio at 3/1. The optimized Pd_3Au_1/AC-THPC catalyst displays the maximum H_2O_2 productivity (165 mol/(kg_{Pd}·h) and selectivity (82.3%) at 10 min. The reduced H_2O_2 productivity and selectivity were observed due to the high H_2O_2 degradation rate under the mild reaction conditions: 1 bar and 10 °C. Its high activity can be maintained for three cycles of reaction. This research would benefit the design of selective bimetallic catalysts.

Supplementary Materials: The following supporting information can be downloaded at https://www.mdpi.com/article/10.3390/catal15060544/s1, Figure S1: TEM micrograph and particle size histogram of Pd-Au/Al_2O_3; Figure S2: The EDX spectra of Pd_3Au_1/AC-THPC catalyst.

Author Contributions: Conceptualization, T.H., B.R., and L.Z.; methodology and investigation, T.H. and L.Z.; data curation, T.H.; and writing, editing, and supervision, B.R. and L.Z. All authors have read and agreed to the published version of the manuscript.

Funding: This research was financially supported by the 2021 Henan Province Colleges and Universities Young Backbone Teacher Training Plan (2021GGJS002), the Henan Major Science and Technology Project (No.221100320100, 221100320200), and the 2021 Nanyang City Collaborative Innovation Major Project (No. 21XTCX12003).

Data Availability Statement: The original contributions presented in this study are included in the article.

Acknowledgments: L.Z. acknowledge the China Scholarship Council for funding.

Conflicts of Interest: Author L.Z. is employed by the company BASF Advanced Chemicals Co., Ltd. The remaining authors declare that the research was conducted in the absence of any commercial or financial relationships that could be construed as potential conflicts of interest.

References

1. Campos-Martin, J.M.; Blanco-Brieva, G.; Fierro, J.L. Hydrogen peroxide synthesis: An outlook beyond the anthraquinone process. *Angew. Chem. Int. Ed.* **2006**, *45*, 6962–6984. [CrossRef]
2. Lewis, R.J.; Hutchings, G.J. Recent advances in the direct synthesis of H_2O_2. *ChemCatChem* **2019**, *11*, 298–308. [CrossRef]
3. Samanta, C. Direct synthesis of hydrogen peroxide from hydrogen and oxygen: An overview of recent developments in the process. *Appl. Catal. A Gen.* **2008**, *350*, 133–149. [CrossRef]
4. Zhang, X.; Xia, Y.; Xia, C.; Wang, H. Insights into practical-scale electrochemical H_2O_2 synthesis. *Trends Chem.* **2020**, *2*, 942–953. [CrossRef]
5. Ranganathan, S.; Sieber, V. Recent advances in the direct synthesis of hydrogen peroxide using chemical catalysis—A review. *Catalysts* **2018**, *8*, 379. [CrossRef]
6. Santos, A.; Lewis, R.J.; Malta, G.; Howe, A.G.; Morgan, D.J.; Hampton, E.; Gaskin, P.; Hutchings, G.J. Direct synthesis of hydrogen peroxide over Au–Pd supported nanoparticles under ambient conditions. *Ind. Eng. Chem. Res.* **2019**, *58*, 12623–12631. [CrossRef]
7. Edwards, J.K.; Solsona, B.E.; Landon, P.; Carley, A.F.; Herzing, A.; Kiely, C.J.; Hutchings, G.J. Direct synthesis of hydrogen peroxide from H_2 and O_2 using TiO_2-supported Au–Pd catalysts. *J. Catal.* **2005**, *236*, 69–79. [CrossRef]
8. Ishihara, T.; Ohura, Y.; Yoshida, S.; Hata, Y.; Nishiguchi, H.; Takita, Y. Synthesis of hydrogen peroxide by direct oxidation of H_2 with O_2 on Au/SiO_2 catalyst. *Appl. Catal. A Gen.* **2005**, *291*, 215–221. [CrossRef]
9. Bu, Y.; Wang, Y.; Han, G.F.; Zhao, Y.; Ge, X.; Li, F.; Zhang, Z.; Zhong, Q.; Baek, J.B. Carbon-based electrocatalysts for efficient hydrogen peroxide production. *Adv. Mater.* **2021**, *33*, 2103266. [CrossRef]
10. Wei, J.; Wang, S.; Wu, J.; Cao, D.; Cheng, D. Progress and perspectives of Pd-based catalysts for direct synthesis of hydrogen peroxide. *Ind. Chem. Mater.* **2024**, *2*, 7–29. [CrossRef]
11. Lopez-Sanchez, J.A.; Dimitratos, N.; Miedziak, P.; Ntainjua, E.; Edwards, J.K.; Morgan, D.; Carley, A.F.; Tiruvalam, R.; Kiely, C.J.; Hutchings, G.J. Au–Pd supported nanocrystals prepared by a sol immobilisation technique as catalysts for selective chemical synthesis. *Phys. Chem. Chem. Phys.* **2008**, *10*, 1921–1930. [CrossRef] [PubMed]
12. Wilson, N.M.; Schröder, J.; Priyadarshini, P.; Bregante, D.T.; Kunz, S.; Flaherty, D.W. Direct synthesis of H_2O_2 on PdZn nanoparticles: The impact of electronic modifications and heterogeneity of active sites. *J. Catal.* **2018**, *368*, 261–274. [CrossRef]
13. Edwards, J.K.; Freakley, S.J.; Carley, A.F.; Kiely, C.J.; Hutchings, G.J. Strategies for designing supported gold–palladium bimetallic catalysts for the direct synthesis of hydrogen peroxide. *Acc. Chem. Res.* **2014**, *47*, 845–854. [CrossRef]

14. Han, Y.-F.; Zhong, Z.; Ramesh, K.; Chen, F.; Chen, L.; White, T.; Tay, Q.; Yaakub, S.N.; Wang, Z. Au promotional effects on the synthesis of H_2O_2 directly from H_2 and O_2 on supported Pd− Au alloy catalysts. *J. Phys. Chem. C* **2007**, *111*, 8410–8413. [CrossRef]
15. Edwards, J.K.; Solsona, B.; Carley, A.F.; Herzing, A.A.; Kiely, C.J.; Hutchings, G.J. Switching off hydrogen peroxide hydrogenation in the direct synthesis process. *Science* **2009**, *323*, 1037–1041. [CrossRef]
16. Edwards, J.K.; Solsona, B.; Landon, P.; Carley, A.F.; Herzing, A.; Watanabe, M.; Kiely, C.J.; Hutchings, G.J. Direct synthesis of hydrogen peroxide from H_2 and O_2 using Au–Pd/Fe_2O_3 catalysts. *J. Mater. Chem.* **2005**, *15*, 4595–4600. [CrossRef]
17. Gao, F.; Goodman, D.W. Pd–Au bimetallic catalysts: Understanding alloy effects from planar models and (supported) nanoparticles. *Chem. Soc. Rev.* **2012**, *41*, 8009–8020. [CrossRef]
18. Morad, M.; Sankar, M.; Cao, E.; Nowicka, E.; Davies, T.E.; Miedziak, P.J.; Morgan, D.J.; Knight, D.W.; Bethell, D.; Gavriilidis, A. Solvent-free aerobic oxidation of alcohols using supported gold palladium nanoalloys prepared by a modified impregnation method. *Catal. Sci. Technol.* **2014**, *4*, 3120–3128. [CrossRef]
19. El Kolli, N.; Delannoy, L.; Louis, C. Bimetallic Au–Pd catalysts for selective hydrogenation of butadiene: Influence of the preparation method on catalytic properties. *J. Catal.* **2013**, *297*, 79–92. [CrossRef]
20. Enache, D.I.; Edwards, J.K.; Landon, P.; Solsona-Espriu, B.; Carley, A.F.; Herzing, A.A.; Watanabe, M.; Kiely, C.J.; Knight, D.W.; Hutchings, G.J. Solvent-free oxidation of primary alcohols to aldehydes using Au-Pd/TiO_2 catalysts. *Science* **2006**, *311*, 362–365. [CrossRef]
21. Rucinska, E.; Pattisson, S.; Miedziak, P.J.; Brett, G.L.; Morgan, D.J.; Sankar, M.; Hutchings, G.J. Cinnamyl alcohol oxidation using supported bimetallic Au–Pd nanoparticles: An optimization of metal ratio and investigation of the deactivation mechanism under autoxidation conditions. *Top. Catal.* **2020**, *63*, 99–112. [CrossRef]
22. Tiruvalam, R.; Pritchard, J.C.; Dimitratos, N.; Lopez-Sanchez, J.A.; Edwards, J.K.; Carley, A.F.; Hutchings, G.J.; Kiely, C.J. Aberration corrected analytical electron microscopy studies of sol-immobilized Au+ Pd, Au {Pd} and Pd {Au} catalysts used for benzyl alcohol oxidation and hydrogen peroxide production. *Faraday Discuss.* **2011**, *152*, 63–86. [CrossRef]
23. Koczkur, K.M.; Mourdikoudis, S.; Polavarapu, L.; Skrabalak, S.E. Polyvinylpyrrolidone (PVP) in nanoparticle synthesis. *Dalton Trans.* **2015**, *44*, 17883–17905. [CrossRef]
24. Rossi, L.M.; Fiorio, J.L.; Garcia, M.A.; Ferraz, C.P. The role and fate of capping ligands in colloidally prepared metal nanoparticle catalysts. *Dalton Trans.* **2018**, *47*, 5889–5915. [CrossRef]
25. Han, G.-H.; Lee, S.-H.; Seo, M.-g.; Lee, K.-Y. Effect of polyvinylpyrrolidone (PVP) on palladium catalysts for direct synthesis of hydrogen peroxide from hydrogen and oxygen. *RSC Adv.* **2020**, *10*, 19952–19960. [CrossRef]
26. Song, B.; Chung, I.; Kim, J.; Yun, M.; Yun, Y. Promoting effects of residual poly(vinyl alcohol) capping agent on the activity and chemoselectivity of Pt/Al_2O_3 for catalytic hydrogenation. *J. Catal.* **2022**, *413*, 614–622. [CrossRef]
27. Cattaneo, S.; Stucchi, M.; Villa, A.; Prati, L. Gold catalysts for the selective oxidation of biomass-derived products. *ChemCatChem* **2019**, *11*, 309–323. [CrossRef]
28. Hueso, J.L.; Sebastián, V.; Mayoral, Á.; Usón, L.; Arruebo, M.; Santamaría, J. Beyond gold: Rediscovering tetrakis-(hydroxymethyl)-phosphonium chloride (THPC) as an effective agent for the synthesis of ultra-small noble metal nanoparticles and Pt-containing nanoalloys. *RSC Adv.* **2013**, *3*, 10427–10433. [CrossRef]
29. Wang, J.; Qiu, X.; Su, K.; Wang, S.; Li, J.; Tang, Y. Breaking the lattice match of Pd on Au (111) nanowires: Manipulating the island and epitaxial growth pathways to boost the oxygen reduction reactivity. *J. Mater. Chem. A* **2020**, *8*, 19300–19308. [CrossRef]
30. Wan, X.; Zhou, C.; Chen, J.; Deng, W.; Zhang, Q.; Yang, Y.; Wang, Y. Base-Free Aerobic Oxidation of 5-Hydroxymethyl-furfural to 2,5-Furandicarboxylic Acid in Water Catalyzed by Functionalized Carbon Nanotube-Supported Au–Pd Alloy Nanoparticles. *ACS Catal.* **2014**, *4*, 2175–2185. [CrossRef]
31. Singh, S.; Bhatnagar, A.; Dixit, V.; Shukla, V.; Shaz, M.A.; Sinha, A.S.K.; Srivastava, O.N.; Sekkar, V. Synthesis, characterization and hydrogen storage characteristics of ambient pressure dried carbon aerogel. *Int. J. Hydrog. Energy* **2016**, *41*, 3561–3570. [CrossRef]
32. Hanrieder, E.K.; Jentys, A.; Lercher, J.A. Interaction of alkali acetates with silica supported PdAu. *Catal. Sci. Technol.* **2016**, *6*, 7203–7211. [CrossRef]
33. Zhu, X.; Guo, Q.; Sun, Y.; Chen, S.; Wang, J.Q.; Wu, M.; Fu, W.; Tang, Y.; Duan, X.; Chen, D.; et al. Optimising surface d charge of AuPd nanoalloy catalysts for enhanced catalytic activity. *Nat. Commun.* **2019**, *10*, 1428. [CrossRef]
34. Wilson, N.M.; Priyadarshini, P.; Kunz, S.; Flaherty, D.W. Direct synthesis of H_2O_2 on Pd and Au_xPd_1 clusters: Understanding the effects of alloying Pd with Au. *J. Catal.* **2018**, *357*, 163–175. [CrossRef]
35. Ouyang, L.; Da, G.-J.; Tian, P.-F.; Chen, T.-Y.; Liang, G.-D.; Xu, J.; Han, Y.-F. Insight into active sites of Pd–Au/TiO_2 catalysts in hydrogen peroxide synthesis directly from H_2 and O_2. *J. Catal.* **2014**, *311*, 129–136. [CrossRef]
36. Tian, P.; Ouyang, L.; Xu, X.; Ao, C.; Xu, X.; Si, R.; Shen, X.; Lin, M.; Xu, J.; Han, Y.-F. The origin of palladium particle size effects in the direct synthesis of H_2O_2: Is smaller better? *J. Catal.* **2017**, *349*, 30–40. [CrossRef]
37. Gu, J.; Wang, S.; He, Z.; Han, Y.; Zhang, J. Direct synthesis of hydrogen peroxide from hydrogen and oxygen over activated-carbon-supported Pd–Ag alloy catalysts. *Catal. Sci. Technol.* **2016**, *6*, 809–817. [CrossRef]

38. Menegazzo, F.; Burti, P.; Signoretto, M.; Manzoli, M.; Vankova, S.; Boccuzzi, F.; Pinna, F.; Strukul, G. Effect of the addition of Au in zirconia and ceria supported Pd catalysts for the direct synthesis of hydrogen peroxide. *J. Catal.* **2008**, *257*, 369–381. [CrossRef]
39. Kanungo, S.; van Haandel, L.; Hensen, E.J.M.; Schouten, J.C.; Neira d'Angelo, M.F. Direct synthesis of H_2O_2 in AuPd coated micro channels: An in-situ X-Ray absorption spectroscopic study. *J. Catal.* **2019**, *370*, 200–209. [CrossRef]
40. Wang, S.; Gao, K.; Li, W.; Zhang, J. Effect of Zn addition on the direct synthesis of hydrogen peroxide over supported palladium catalysts. *Appl. Catal. A Gen.* **2017**, *531*, 89–95. [CrossRef]
41. Wang, S.; Lewis, R.J.; Doronkin, D.E.; Morgan, D.J.; Grunwaldt, J.-D.; Hutchings, G.J.; Behrens, S. The direct synthesis of hydrogen peroxide from H_2 and O_2 using Pd–Ga and Pd–In catalysts. *Catal. Sci. Technol.* **2020**, *10*, 1925–1932. [CrossRef]
42. Asad, S.; Torabi, S.-F.; Fathi-Roudsari, M.; Ghaemi, N.; Khajeh, K. Phosphate buffer effects on thermal stability and H_2O_2-resistance of horseradish peroxidase. *Int. J. Biol. Macromol.* **2011**, *48*, 566–570. [CrossRef] [PubMed]